# JMB

# Modulation of Glycophorin A Transmembrane Helix Interactions by Lipid Bilayers: Molecular Dynamics Calculations

## Horia I. Petrache[1], Alan Grossfield[2], Kevin R. MacKenzie[3] Donald M. Engelman[3] and Thomas B. Woolf[1,2]*

[1]*Department of Physiology and*

[2]*Department of Biophysics Johns Hopkins University School of Medicine, Baltimore MD 21205, USA*

[3]*Department of Molecular Biophysics and Biochemistry Yale University, New Haven CT 06520, USA*

Starting from the glycophorin A dimer structure determined by NMR, we performed simulations of both dimer and monomer forms in explicit lipid bilayers with constant normal pressure, lateral area, and temperature using the CHARMM potential. Analysis of the trajectories in four different lipids reveals how lipid chain length and saturation modulate the structural and energetic properties of transmembrane helices. Helix tilt, helix-helix crossing angle, and helix accessible volume depend on lipid type in a manner consistent with hydrophobic matching concepts: the most relevant lipid property appears to be the bilayer thickness. Although the net helix-helix interaction enthalpy is strongly attractive, analysis of residue-residue interactions reveals significant unfavorable electrostatic repulsion between interfacial glycine residues previously shown to be critical for dimerization. Peptide volume is nearly conserved upon dimerization in all lipid types, indicating that the monomeric helices pack equally well with lipid as dimer helices do with one another. Enthalpy calculations indicate that the helix-environment interaction energy is lower in the dimer than in the monomer form, when solvated by unsaturated lipids. In all lipid environments there is a marked preference for lipids to interact with peptide predominantly through one rather than both acyl chains. Although our trajectories are not long enough to allow a full thermodynamic treatment, these results demonstrate that molecular dynamics simulations are a powerful method for investigating the protein-protein, protein-lipid, and lipid-lipid interactions that determine the structure, stability and dynamics of transmembrane α-helices in membranes.

© 2000 Academic Press

*Keywords:* glycophorin A transmembrane domain; membrane proteins; protein-lipid interactions; α-helix association; dimerization motif

*\*Corresponding author*

## Introduction

A large fraction of membrane proteins consist of bundles of transmembrane α-helices. Despite their abundance, the process by which these bundles form is not well understood. One possible mechanism for helix association of membrane proteins is the two-stage folding model proposed by Popot & Engelman (1990; see also Engelman & Steitz, 1981). In this framework, the transmembrane helices first form independently, then pack together into a stable tertiary structure. The transmembrane domain of glycophorin A (GpA) is an excellent model system for the study of transmembrane helix association (Bormann & Engelman, 1992; Lemmon & Engelman, 1994). GpA contains a single transmembrane helix, and forms a homodimer under native conditions.

The GpA dimer structure was first predicted computationally, by Treutlein *et al.* (1992), using the results of extensive mutagenesis work (Lemmon *et al.*, 1992a,b) to narrow the search. The

prediction was later refined, using an improved global search method (Adams *et al.*, 1996). More recently, the structure of the GpA dimer in dodecyl phosphocholine micelles was determined using NMR measurements (MacKenzie *et al.*, 1997). The close agreement between the experimental and computational results indicated that computational approaches can be powerful tools for understanding membrane proteins, especially when combined with preliminary experimental results.

The previous GpA structure calculations focused entirely on protein-protein interactions, and completely neglected the interactions between the protein and the micelle or the lipid bilayer. By contrast, simulations of soluble proteins have consistently demonstrated the importance of solvent in obtaining reasonable structures and dynamics (Novotny *et al.*, 1984; Brooks *et al.*, 1988). The environment effect is likely to be even more pronounced in the case of membrane proteins, since lipid bilayers are strongly anisotropic and therefore greatly restrict protein motions.

Lipid properties have been shown to modulate protein folding, structure, and function in many membrane systems. For example, the role of lipid headgroup, chain length and unsaturation on the photochemical behavior of rhodopsin has been documented by Brown (1994) and Litman & Mitchell (1996). Koeppe and collaborators have shown the dependence of gramicidin conformation on lipid chain length, and identified a minimal threshold for channel formation (Greathouse *et al.*, 1994; Koeppe & Andersen, 1996). The role of headgroup interactions has been studied by Gawrisch *et al.* (1993) in the case of the P828 peptide fragment from the envelope glycoprotein gp41, while Bezrukov *et al.* (1998) have determined the effect of lipid packing on alamethicin channel formation and conductance. Many other examples can be found in recent reviews by Killian (1998), Epand (1998), and White & Wimley (1999).

A large body of experimental work has suggested that lipid properties are in turn modified by the presence of the protein (Pink *et al.*, 1981; Keller *et al.*, 1996; de Planque *et al.*, 1998). In particular, a hypothesis has been proposed that boundary lipids next to the protein are more strongly perturbed than are the lipids further removed from it (Jost *et al.*, 1973). However, the range of this perturbation effect on the lipid bilayer, as well as the precise effect on the protein or peptide remain uncertain (Rehorek *et al.*, 1985; Sperotto & Mouritsen, 1991; Chiu *et al.*, 1999; Harroun *et al.*, 1999), and therefore require more investigation.

In general, structural studies of membrane proteins are a challenge even for modern experimental techniques, owing to the difficulty of obtaining appropriate samples for X-ray diffraction and NMR spectroscopy (Fu & Cross, 1999). Nonetheless, it is hoped that a combination of experimental and theoretical approaches will lead to a full thermodynamic description of the membrane protein system (White & Wimley, 1999). To be complete, such a thermodynamic description should include information not only about the average protein structure, but also about the range of fluctuations about this average. In this context, computer simulations have become indispensable tools for solving and understanding complex molecular systems (Brooks *et al.*, 1988). All-atom simulations, which include the lipid bilayer explicitly, are able to give detailed information on both protein and lipid molecules. This approach, while computationally expensive, can help elucidate the precise mechanism by which the lipid bilayer influences the protein free energy surface.

Molecular dynamics simulations of transmembrane domains in explicit lipid bilayers are becoming more common. In one of the earlier efforts, Edholm *et al.* (1995) simulated a bacteriorhodopsin trimer in an explicit lipid bilayer and studied environmental effects on the protein structure and fluctuations. Woolf & Roux (1994, 1996) performed simulations of gramicidin A channel, and of Pf1 coat protein (Roux & Woolf, 1996), and showed the reciprocal effect of the interacting peptide and lipids on their dynamic structure. A recent simulation of gramicidin A by Chiu *et al.* (1999) focused on the boundary lipids and reported an increased bilayer thickness adjacent to the gramicidin channel and correspondingly, increased acyl chain order parameters. Stouch and co-workers simulated a polyalanine peptide (Shen *et al.*, 1997), while a number of lipid/protein systems have been analyzed in a series of papers from Berendsen's and Sansom's groups and are summarized by Tieleman *et al.* (1998).

The present set of molecular dynamics calculations addresses the effects of the lipid environment on the GpA transmembrane structure and dynamics, and, in general, the issue of lipid-peptide interactions in fluid phase lipid bilayers. The focus of this paper is on helix association, the second stage of the Popot-Engelman model, which occurs entirely within the lipid bilayer environment. This study does not therefore discuss the helix insertion/formation mechanism, assumed to occur in an earlier distinct stage. We have considered four different lipid types in an attempt to examine the influence of various lipid properties. The first two of the lipids, dimyristoyl-phosphatidylcholine (DMPC) and dipalmitoyl-phosphatidylcholine (DPPC), have two saturated acyl chains. The third, dioleoyl-phosphatidylcholine (DOPC) has two unsaturated chains with one double bond at position 9, while the fourth, 1-palmitoyl-2-oleoyl-phosphatidylcholine (POPC), has one saturated and one unsaturated chain. All lipids considered have a phosphocholine (PC) headgroup. With this minimal set of lipids we attempt to monitor GpA behavior as a function of lipid chain length and saturation. In addition, the POPC runs provide a comparison with mixed-chain systems. Each system consists of a GpA monomer or dimer and 30 lipid molecules. The number of

water molecules in each case was chosen based on experimental measurements of fully hydrated multilamellar vesicles of pure lipid bilayers, as described in Methods.

In the framework of the two-stage model, we have simulated both monomer and dimer forms of GpA for the purpose of understanding the role of helix-lipid interactions in the stability of helix association. The goal of this paper is to set the basis for a long term systematic investigation of environmental effects on the structure, dynamics, and pair association of the GpA transmembrane domain.

## Structural Results

The analysis of an extensive set of molecular dynamics simulations of the glycophorin transmembrane domain in explicit bilayers is reported. Both GpA monomer and dimer were simulated in four different lipid bilayer environments, for a total of eight independent simulations. In each case, simulations of 1.5 ns duration were completed and analyzed. The results suggest, at least at this time-scale, modulation of GpA behavior by the lipid environment.

The simulation results indicate that the trajectories sample an equilibrium population of states in the vicinity of their starting conformation, and that no dramatic (systematic) drift of the properties of interest has occurred, after an initial equilibration window for each trajectory. While it is difficult to prove that a molecular dynamics simulation is fully equilibrated at all time scales and for all degrees of freedom, certain properties have traditionally been used in an effort to check for reasonable behavior. A necessary test is the stability of the trajectory, as an indication that a well defined region in phase space was sampled, and that simulation settings were compatible with the structure of interest. In this regard, Figure 1(a) shows the box dimension along the bilayer normal as a function of simulation time for the GpA/DMPC simulations. Since the lateral box dimensions were kept constant (see Methods), the time series shown represent the simulation box volumes, up to a factor equal to the lateral area in each case. Furthermore, all of the current simulations reached stable, well-defined GpA conformations after about 250 ps of full dynamics (see Methods for a description of earlier equilibration stages involving restraints). This is demonstrated by the root-mean-square (RMS) deviations of GpA backbone atoms and by the dynamics of backbone dihedrals. The RMS deviations, shown in Figure 1(b) for a representative trajectory, are calculated relative to the first structure after 250 ps of trajectory production. For all trajectories, the RMS deviations remained below 1.5 Å throughout the subsequent 1.25 ns simulation times. With regard to equilibration, additional properties are pre-
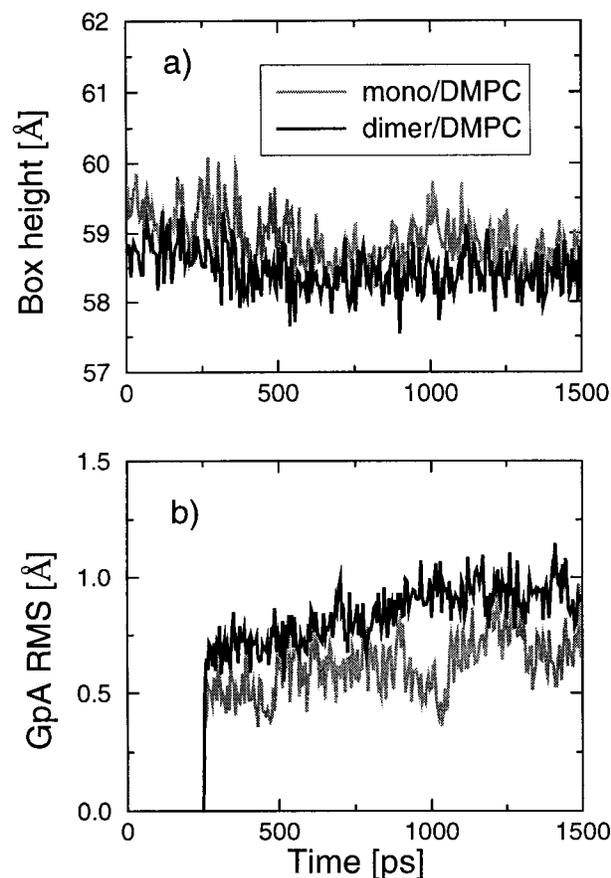


**Figure 1.** (a) Time course of box dimension along the bilayer normal for the GpA/DMPC simulations. (b) Root-mean-square (RMS) deviations for GpA backbone atoms in the DMPC trajectories. Global GpA translation and rotation are removed. The RMS deviations are calculated relative to the structure at 250 ps, as explained in the text.

sented throughout the paper, in particular when helix tilt and helix-lipid packing are discussed.

### Transmembrane domain structural properties

A first description of the trajectory-averaged GpA structure is given in Figure 2, where we show the average values and fluctuations of backbone dihedral angles. Despite large fluctuations (as indicated by the vertical bars in Figure 2) the average backbone structure remained in a stable α-helical conformation for both monomer and dimer forms. As expected, backbone fluctuations and deviations from ideal α-helix dihedral values were found to be greater at the helix ends than at the helix center (similar behavior was observed in the molecular dynamics simulations of individual bacteriorhodopsin helices in DMPC (Woolf, 1997)). This is especially true in the dimer simulations, where, as we show later, the individual helices are more tilted relative to the bilayer normal than in the single monomer form. Also note that the Ψ dihe-
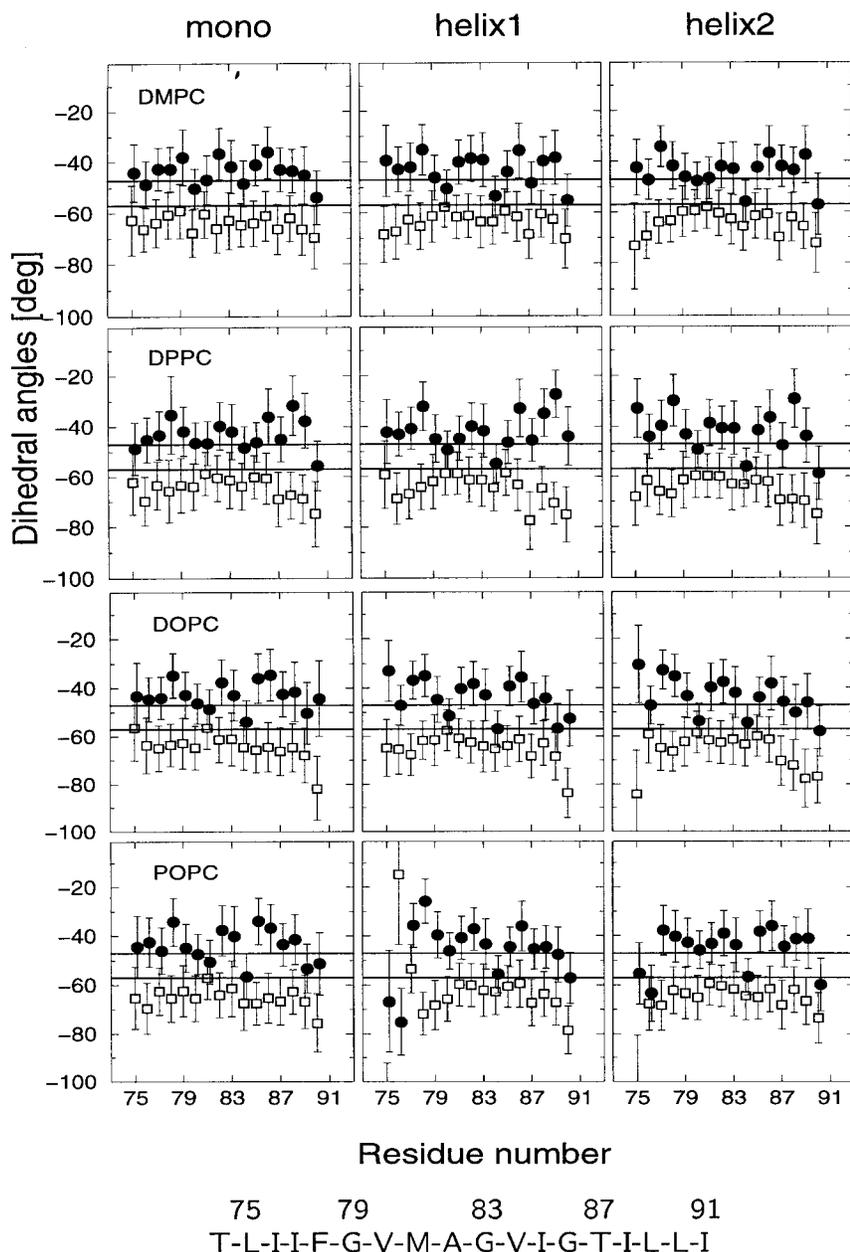
**Figure 2.** Backbone $\Phi$-$\Psi$ dihedral angles (shown with open squares and filled circles, respectively), for monomer and dimer helices. The four solvent media are shown. The error bars represent the root-mean-square fluctuations for the simulated dynamics. The continuous lines at $-47$ and $-57$ degrees on each panel represent ideal $\alpha$-helix values.

dral angles of valine residues (especially V84) next to glycine residues are more negative in the dimer form. Within the conformational space sampled in each simulation, different average values and fluctuations are observed: the structure adopted by the backbone dihedrals is not exactly identical in each environment. Although statistical significance is uncertain due to limited sampling, these differences suggest that the environment modulates the subspace of structurally accessible states during GpA thermal motion, and this fact should be reflected in measurements of thermodynamic parameters. Note that among the four lipid types, the POPC simulation shows a more pronounced dis-

tortion of the N terminus, giving an early indication that the sampled GpA dynamics in POPC may be significantly different than in the other simulations. This fact is discussed in more detail in Interaction Results.

Of special interest regarding the dimer structure is the nature of the helix-helix interface. A detailed description of the dimer structure observed in each environment is provided by a matrix of distances between residue pairs on the two opposed helices. The trajectory averaged distances are presented in Figure 3 as grey scale grids. The darker patterns, representing close residue-residue contacts, identify the motif sequence xLIxxGVxxGVxxT, located
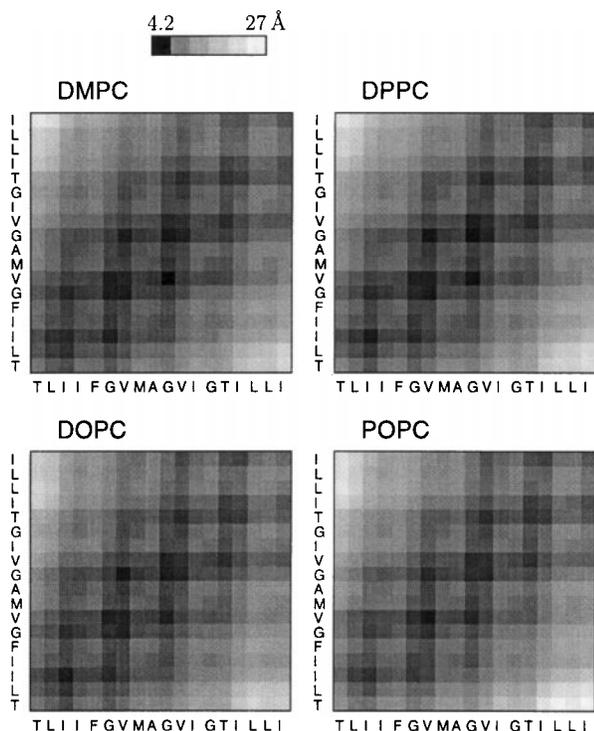
**Figure 3.** Residue-residue distance matrix between $C^\alpha$ atoms in the dimer form. The distances vary between 4.2 Å (dark fill) and 27 Å (white fill). The intermediate gray levels have been assigned using a square root functional form for better contrast.

at the dimer interface. These are precisely the critical residues identified by mutagenesis studies (Lemmon *et al.*, 1992a,b). The observed inter-residue distances are the result of intermolecular interactions that dictate the relative helix-helix orientation. One direct observation from Figure 3 is the symmetry of the patterns in each trajectory. This symmetric pattern indicates a symmetric helix-helix orientation, and in particular, a negligible shift along the helical axes in agreement with Adams *et al.* (1996).

A number of trajectory-averaged geometrical parameters that describe global helix orientation are summarized in Table 1. The root-mean-square deviations for each parameter are also given in order to emphasize the range of fluctuations present in the simulated dynamics. The center of mass (CM) separations were calculated based on all helix atoms, including hydrogens. Helix orientation (tilt) was obtained by finding the axis of a cylindrical surface that best fit the α-carbon atoms in each helix (CHARMM subroutine; using the method of Chothia *et al.*, 1981). With this approach, a unit vector is assigned to each helix in each frame. The dimer tilt is then defined as the orientation of the vector sum of individual monomer unit vectors, and the helix crossing angle ($\Omega$) as the angle between them. Table 1 shows that there is a greater

helix separation in the case of POPC, and a larger crossing angle in DMPC. For the dimer tilt, a lower value is seen in DOPC. Interestingly, dimer tilt (as a whole) relative to the bilayer normal is similar in magnitude and fluctuations with the monomer tilt (in the monomer trajectories), despite the fact that the dimer has greater cross-sectional area. However, the tilt angle for each individual monomer in the dimer form is much larger in magnitude, as shown for a typical trajectory (DMPC) in Figure 4. In addition, it is apparent from the time series presented in Figure 4 that the tilt angles of the two monomers are anticorrelated, meaning that the dimer tilts preferably in the dimer plane (perpendicular to the line that connects the centers of the two helices).

**Lipid bilayer structure**

The structure of the lipid bilayer itself is altered by the presence of the protein. One important structural parameter is the distance between the lipid headgroups ($D_{HH}$) across the bilayer. This distance can be measured experimentally using X-ray scattering, and represents a measure of the bilayer thickness (Lewis & Engelman, 1983). Because the lipid electron density is concentrated at the phosphorus atom (P), the measured $D_{HH}$ is approximately given by the distance between the average location of the P atoms in the two monolayers ($D_{PP}$). In Table 2 we report $D_{PP}$ values from our GpA/lipid simulations and compare them with our neat bilayer simulations (with similar boundary conditions and system sizes), and with experimental $D_{HH}$ data from fully hydrated lipid samples, at the same temperatures as the simulated trajectories.
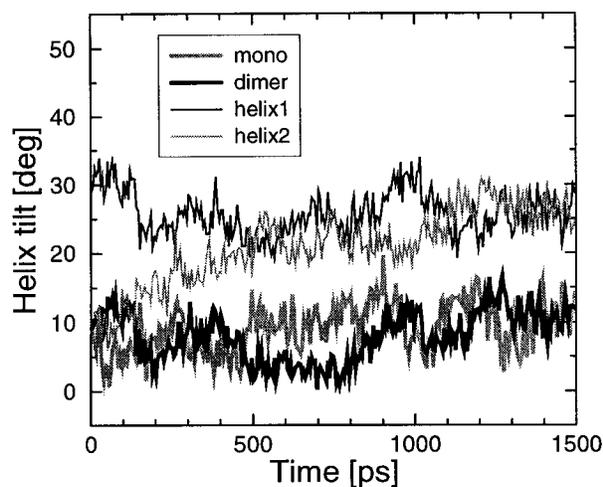


**Figure 4.** Time series of helix tilt from the GpA/DMPC trajectories. The time series shown include the initial 250 ps equilibration window. The thick grey line shows the monomer trajectory. The thick black line shows the global dimer tilt, and the thin lines each show individual monomers in the dimer trajectory.

**Table 1.** Helix orientation parameters

| Lipid | CM (Å) | $\Omega$ (deg.) | Dimer tilt (deg.) | Mono tilt (deg.) |
|---|---|---|---|---|
| DMPC | $8.2 \pm 0.3$ | $-46 \pm 4$ | $8 \pm 4$ | $10 \pm 3$ |
| DPPC | $8.1 \pm 0.2$ | $-39 \pm 3$ | $9 \pm 2$ | $9 \pm 3$ |
| DOPC | $8.4 \pm 0.2$ | $-41 \pm 3$ | $6 \pm 2$ | $8 \pm 4$ |
| POPC | $9.4 \pm 0.3$ | $-40 \pm 3$ | $11 \pm 3$ | $9 \pm 3$ |

Center of mass separation (CM), crossing angle ($\Omega$), global dimer tilt, and monomer tilt (from monomer trajectories). Average values and fluctuations over the trajectories are shown.

As a general trend, the bilayer thicknesses in the dimer simulations are smaller than in the monomer simulations. While this can be explained by the larger perturbation imposed by the presence of the helix dimer, it is worth checking that the result is not an artifact due to our choice of the lateral area. A first indication would be the presence of unreasonable values for the surface tension. The last two columns in Table 2 show the calculated surface tensions for each run, as given by the CHARMM output (method by Zhang *et al.*, 1995). These values for the surface tension are typical for simulations of lipid bilayer systems (Feller *et al.*, 1997; Feller & Pastor, 1999). Due to the small system size, the fluctuations in the surface tension are very large. Fluctuations between 50 ps block averages gave RMS deviations of about 20 dyn/cm for the monomer trajectories, and slightly smaller, of about 15 dyn/cm for the dimer trajectories. For nanosecond time scales, differences on the order of 10 dyn/cm in the surface tension are not expected to cause significant changes in the bilayer structure (Feller & Pastor, 1999). The fact that the magnitude of the surface tensions observed are reasonable, and that the differences between the monomer and dimer simulations are barely resolvable suggest that the simulated lipid bilayers are, at least in a first approximation, under similar lateral stress. Therefore, the results presented in Table 2 indicate that the lipid bilayer thickness decreases upon GpA dimerization. We emphasize, however, that the magnitude of the effect may depend on the precise values of the boundary conditions.

Besides the average thickness, of special interest is the local effect of GpA on the lipid bilayer. The boundary $D_{PP}$ values are shown in parentheses in Table 2, next to the average values. With an error margin of 0.5 Å, we find that the boundary thickness is larger for the monomer, but smaller for the dimer simulations when compared to the average values in each case. This suggests that the effect on the boundary lipids depends on the size of the embedded molecule. Indeed, Tieleman *et al.* (1998) showed that while membrane insertions almost always influence the bilayer structure, the effects vary with the properties of the inserted molecule. A systematic study of WALP/lipid systems (Petrache *et al.*, 2000) shows that hydrophobic matching is a complex mechanism that involves a large number of degrees of freedom. Besides the basic peptide and lipid lengths (static properties), the peptide and lipid tilt (dynamic properties) are relevant.

### GpA-lipid packing

The GpA structure and the structure of the lipid bilayer are coupled through intimate molecular packing. One measure of the lipid-protein packing is the available volume for each molecular component of the system. For heterogenous systems, these volumes can be calculated from simulations using the Voronoi method (Richards, 1985). We have used the program developed by Gerstein *et al.* (1995) to first calculate the accessible volumes for all GpA heavy atoms (see Methods). The volumes for individual atoms were then summed to obtain

**Table 2.** Lipid bilayer parameters

| Lipid | $D_{HH}^{neat}$ (exp) | $D_{PP}^{neat}$ | $D_{PP}^{mono}$ | $D_{PP}^{dimer}$ | $\Delta D_{PP}/D_{PP}$ | $\gamma_{neat}$ | $\gamma_{mono}$ | $\gamma_{dimer}$ |
|---|---|---|---|---|---|---|---|---|
| DMPC | 34.4[a] | 35.9 | 33.8 (33.0) | 32.5 (33.8) | $-3.8\%$ | 21 | 29 | 47 |
| DPPC | 36.4-39.6[b] | 39.0 | 36.1 (35.0) | 34.4 (35.4) | $-4.7\%$ | 44 | 35 | 27 |
| DOPC | 35.3[c] | - | 35.0 (35.0) | 33.2 (33.8) | $-5.1\%$ | - | 15 | 12 |
| POPC | - | - | 37.8 (36.3) | 35.4 (35.1) | $-6.3\%$ | - | 24 | 19 |

Experimental $D_{HH}^{neat}$ are from measurements on pure lipid bilayers at full hydration and in the fluid lamellar phase (temperatures were 30 °C for DMPC and DOPC, and 50 °C for DPPC). Average $D_{PP}$ distances are calculated from simulations, as explained in the text (simulations of neat DOPC and POPC were not performed, therefore we report $D_{PP}^{neat}$ for DMPC and DPPC only). The numbers in parentheses give the bilayer thickness for boundary lipids. Column 6 gives the percentage change of average $D_{PP}$ between the monomer and the dimer trajectories. The last three columns give the surface tension (in units of dyn/cm) calculated from the trajectories.
[a] Petrache *et al.* (1998a).
[b] Nagle *et al.* (1996).
[c] Tristram-Nagle *et al.* (1998).

the total helix volumes. Table 3 gives the total volumes for GpA determined by this method in each lipid bilayer.

Compared to the bare van der Waals volumes, of about 2260 Å$^3$ per GpA monomer, the thermally accessible volumes are larger by approximately 25 %. While the precise results depend on the choice of the Voronoi dividing planes (Gerstein *et al.*, 1995), it is clear that the helix volume changes upon dimerization are of the order of 1 % or less. At atmospheric pressure, the $P\Delta V$ term in the free energy of helix-helix association is negligible ($P\Delta V \leqslant 1$ cal/mol). In addition, we have estimated the overall volumetric changes upon dimerization by comparing the total volume from the monomer simulations and an adjusted volume from the dimer simulations. The adjustment in the case of the dimer consists in subtracting out one monomer and the corresponding number of water molecules, in order to have the same GpA-monomer/lipid/water ratios as in the monomer systems. We obtained volume changes of the order of 0.1 % which are at the limit of the simulation resolution. The small volume difference indicates that optimal lipid packing around the GpA peptide can be almost equally achieved in both monomer and dimer form, and in addition, that molecular packing at the helix-helix interface conserves the available volume. The volumes per lipid molecule, calculated by subtracting the peptide and the water volumes from the total volume of each simulation box are also shown in Table 3. The lipid volume results agree with former calculations (Petrache *et al.*, 1997; Armen *et al.*, 1998) and experimental measurements (Nagle *et al.*, 1996; Petrache *et al.*, 1998a; Tristram-Nagle *et al.*, 1998) and show no significant change with peptide insertion.

The molecular packing inside the lipid bilayer, and in particular the precise value of the helix volume depends on many factors. The most important of these factors is the density gradient along the bilayer normal (Wiener & White, 1992; Petrache *et al.*, 1997; Armen *et al.*, 1998). Due to this density gradient, the accessible helix volumes are controlled by an interplay between helix tilt and bilayer thickness. For example, as shown in Table 3, the percentage change in helix volume upon dimerization is much smaller in DMPC, which has the smallest bilayer thickness (see

Table 2), than in the other three lipids. Specifically, the bilayer thickness decreases from 33.8 Å in the mono/DMPC trajectory to 32.5 Å in the dimer/DMPC trajectory, approaching the GpA helix length of roughly 32 Å. The small bilayer thickness might be the reason why the helix crossing angle is larger in DMPC than in the other bilayers. The larger crossing angle, in turn, results in an increase in helix volume upon dimerization. Moreover, the GpA volume is lowest in the DOPC trajectories, despite the greater area of the simulation box (see Table 6, below). However, both the GpA tilt and the bilayer thickness are small in the DOPC trajectories, thus implying that the helix ends explore regions of higher density near the lipid glycerol backbone. Also note that the POPC trajectories have larger volumes than DOPC. This is related to the greater bilayer thickness and the larger inter-helical distance (see Table 1) in this case.

Another important aspect of the peptide-lipid packing is the extent of fluctuations in the helix volume. A first observation is that the volume fluctuations of the two monomers in the dimer form are roughly uncorrelated, as indicated by the fact that the fluctuations at dimer level scale as $1/\sqrt{2}$ relative to the fluctuations at monomer level. The absence of correlation between monomeric units is better seen in Figure 5, which shows the distribution of monomer volumes from a representative dimer simulation. A second observation is that, when comparing the different lipid types, the GpA volume fluctuations decrease upon dimer formation, in the case of the two unsaturated, as opposed to the two saturated lipids. We note that, in terms of solvent (hydrocarbon) volume units, the magnitude of GpA volume fluctuations and changes upon dimerization are comparable with the volume of two methylene groups (CH$_2$) in the lipid acyl chains. The lipid methylene volume in the fluid phase, was determined to be about 28 Å$^3$ from both specific volume measurements (Nagle & Wilkinson, 1978) and lipid bilayer simulations (Petrache *et al.*, 1997; Armen *et al.*, 1998). This connection between the peptide volume changes and solvent volumes was found to be relevant for estimating the energetic cost of packing defects in lipid bilayers. For example, it has been estimated that a free energy of about 1.6 kcal/mol is required

**Table 3.** Thermally accessible volumes calculated using the Voronoi procedure

| Lipid | $V_m$ | $V_d/2$ | $\Delta V/V$ (%) | $V_L^{\text{neat}}$ | $V_L^{\text{mono}}$ | $V_L^{\text{dimer}}$ |
|-------|-------|---------|------------------|---------|---------|---------|
| DMPC | 2806 ± 44 | 2809 ± 47 (37) | 0.1 | 1085 | 1089 | 1094 |
| DPPC | 2848 ± 48 | 2815 ± 47 (36) | −1.1 | 1223 | 1219 | 1224 |
| DOPC | 2794 ± 50 | 2766 ± 43 (33) | −1.0 | - | 1298 | 1294 |
| POPC | 2831 ± 53 | 2799 ± 44 (33) | −1.1 | - | 1251 | 1256 |

$V_m$ represents the monomer volume in the monomer simulations. The dimer values (denoted by $V_d/2$) represent the average volume per monomer and the volume fluctuations at monomer level, in the dimer simulations. The values in parentheses give the volume fluctuations at dimer level. Column 4 gives the percentage change in volume per monomer upon dimer formation. The last three columns give the volume per lipid molecule ($V_L$) calculated from each simulation. For each lipid, volume variations among different simulations are less or about 0.5 %. The volume units are Å$^3$.
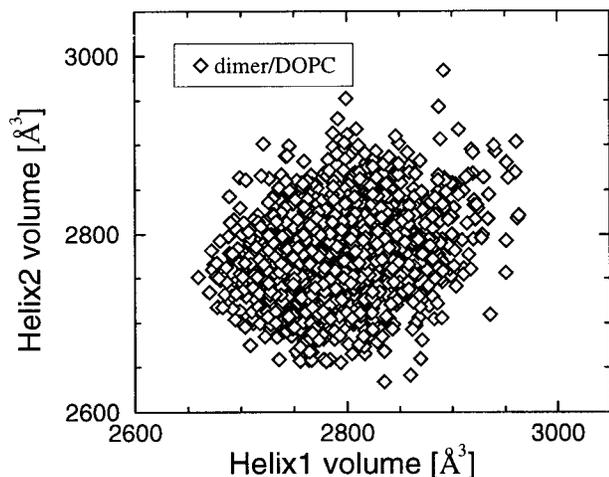
**Figure 5.** Instantaneous monomer volumes from the GpA dimer/DOPC simulation.

to create a void volume comparable with twice the lipid methylene volume (White & Wimley, 1999).

In order to give a more detailed description of the GpA-lipid packing, we examined volumetric values at the residue level, as shown in Figure 6. The reported residue volumes do not include the atoms involved in the peptide bond (N, HN, C, and O), but include the backbone α-carbon atoms. For example, the reported glycine volumes rep-resent the $C^{\alpha}H_2$ groups. We note that the smaller residues (G79, G83, G86, as well as A82) show no significant volume changes between the monomer and the dimer forms. More importantly, all three glycine residues have the same volume, regardless of their location relative to the dimer interface, and in addition, their magnitude is practically equal to the volume of the methylene group in the lipid hydrocarbon chains.

The largest accessible volumes seen in Figure 6 correspond to the aromatic phenylalanine side-chains (F78). These residues are located on the side opposite to the helix-helix interface, and are there-fore in direct contact with the lipids surrounding the dimer. On average, the F78 side-chains are located inside the lipid hydrocarbon region closer to the lipid carbonyls. The volumes of F78 side-chains are of about 173 $Å^3$ and are comparable in magnitude with the volumes of lipid headgroup fragments, which for DPPC at 50 °C are 173 $Å^3$ for carbonyls + glycerol and 153 $Å^3$ for phosphate + choline (Petrache *et al.*, 1997; Armen *et al.*, 1998). Recent studies by Yau *et al.* (1998) have demon-strated the preference of aromatic groups for the heterogeneous environment of the lipid-water interface. This suggests that the location of F78 along the bilayer normal (*z*-axis) is an important factor in determining the equilibrium location and orientation of the GpA molecule. Figure 7 shows the F78 center of mass location within the bilayer as a function of simulation time. The center of the membrane (i.e. the $z = 0$ level) has been set at the
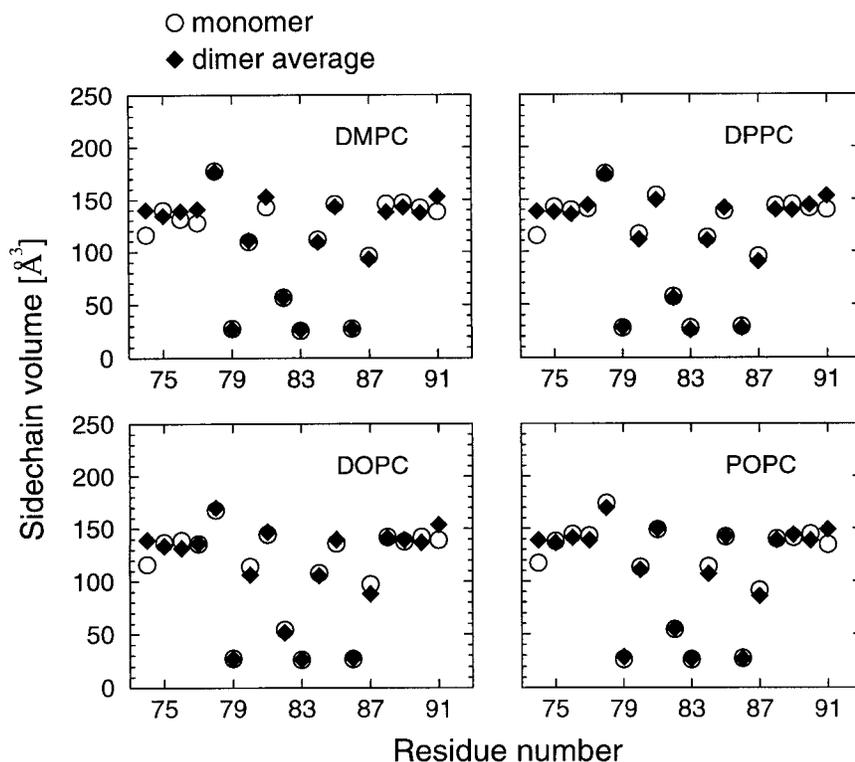


**Figure 6.** Trajectory averaged side-chain volumes (include the backbone $C^{\alpha}$ and do not include the peptide bond atoms N, HN, C, or O). Monomer is shown with open circles, and dimer is shown with filled diamonds.
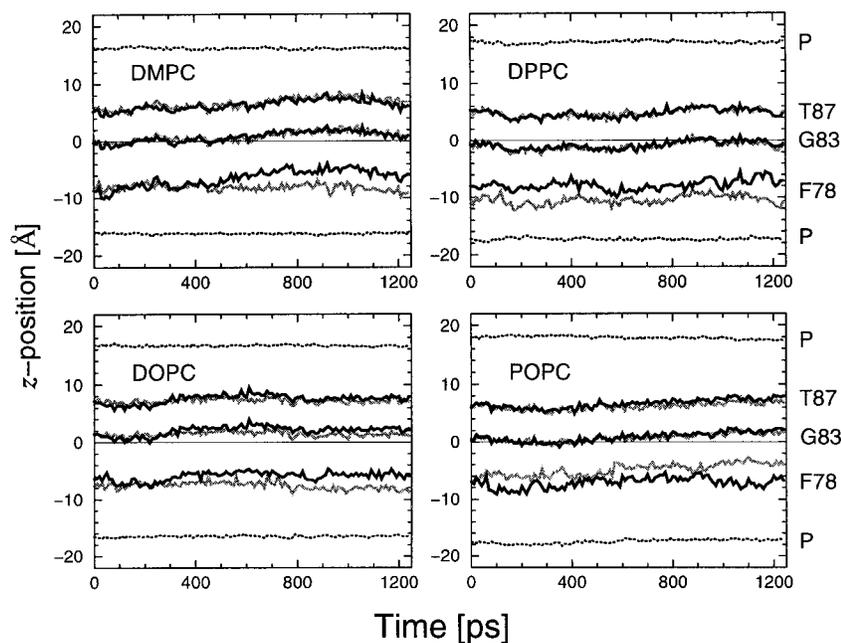
**Figure 7.** Center of mass location along the bilayer normal for the F78, G83, and T87 side-chains (backbone atoms not included except for $C^{\alpha}$). Trajectories from residues on each of the two helices in the dimer form are shown with different line types. The dotted curves represent the average positions of lipid phosphorus atoms (P) for each monolayer (averaged over all lipids in each frame).

center of mass of the lipids. Figure 7 also shows the locations of G83 and T87 side-chains, and the average positions of the lipid phosphorus atoms, in order to give a reference for the GpA orientation within the lipid bilayer. Among the residues shown, G83 is located at the bilayer center, while F78 and T87 are closer to the lipid headgroup regions. It is important to note that, while the average position of lipid phosphorus atoms is practically constant during the simulation, individual lipid molecules undergo significant vertical motion generating a distribution of the P atoms with a width of 3-5 Å (not shown).

The time series presented in Figure 7 reveal important aspects of the simulated dynamics. First, the constancy of the bilayer thickness ($D_{PP}$) during the analyzed trajectories confirms the global stability of the membrane system. Second, the locations of the GpA residues along the bilayer normal indicate a rigid body motion of the dimer of roughly 2 Å amplitude, within the nanosecond simulation time. Third, faster fluctuations are observed about this slow rigid body motion for all systems. Altogether, these results indicate a degree of motional coupling between the two α-helices in the dimer, as a consequence of the strong helix-helix interactions discussed in the next section.

Finally, we note that the two F78 residues of the GpA dimer are sampling slightly different environments. This is due to the particular way the dimer is tilted relative to the bilayer normal (*vide supra*). A fully converged molecular dynamics trajectory (probably on microsecond or millisecond time scales) would presumably show a more symmetric ensemble of states between the two chemically equivalent monomers. We emphasize that in addition to the motion along the *z*-axis, there is a significant degree of motion of the GpA peptide in

the membrane plane, that is not captured in Figure 7.

## Interaction Results

The structural parameters analyzed in the previous sections are determined by the net balance of complex molecular interactions. The number of relevant energy terms required for a complete thermodynamic description of a peptide/lipid bilayer system is quite large as emphasized by White & Wimley (1999). These terms include intra and inter-molecular interactions (enthalpies) as well as entropic terms. The formation and stability of the peptide secondary structure involves an energetic balance between residue-residue interactions in the polypeptide chain and interactions with the solvent environment (Kovacs *et al.*, 1995). While inter-molecular interactions characterize the association of various molecular species, the intra-molecular (self) energies measure the deformations (strains) imposed on the molecular structure by these associations. For example, the lipid/water molecules may distort the peptide α-helical structure, and do this differently for an isolated helix than for a helix pair. In addition, the process of helix association itself may distort the secondary structure of the dimer units and further alter helix self energy.

Given that the entropic terms are not easily within reach, in what follows we discuss trajectory averaged interaction energies (enthalpic terms) between the GpA peptide and the membrane environment in order to describe how different molecular constituents are coupled within the simulations. We shall first present intra-helical interactions (responsible for secondary structure formation and stability), followed by direct helix-

helix interactions. We then turn to helix-environment and environment-environment interactions.

## Intra and inter-helical interactions

The intra-helical interactions ($H_{intra}$) per GpA monomer are shown in Table 4, and are decomposed into contributions from non-bonded (van der Waals and electrostatic) and bonded terms. The latter include energies associated with bond length and angle distortions and are basically set by the simulation temperature, as can be seen by comparing the DPPC run at 50 °C with the other three runs at 30 °C. The net change in intra-helical interactions ($\Delta H_{intra}$) is given in column 6 of Table 4 and appears to be marginal (estimated error is 1 kcal/mol), except in the case of the POPC simulation which shows a significantly higher helix self energy for the dimer form.

For a detailed analysis of inter-helical interactions, we computed interaction energies between inter-molecular residue pairs of the dimer. Each lipid environment, in principle, can interact differently with the GpA dimer and modulate inter-helical conformations. This fact is revealed in Figure 8, where we present the residue-residue interaction matrices for all dimer trajectories. The residue interaction terms include side-chain as well as backbone atoms. Most residue-residue interactions are attractive, with values between −2.5 kcal/mol and zero, except for a number of glycine-glycine interactions that are repulsive, and are marked by the plus signs in Figure 8. The repulsive component in the glycine-glycine interactions is mostly given by the unfavorable electrostatic interactions between both backbone carbonyls and the $C^{\alpha}H_2$ groups. The magnitude of the overall glycine-glycine interactions is between 0.1 and 0.5 kcal/mol, with the variations depending on the glycine location (G79 or G83) and on the lipid type. Similar to the distance matrix (Figure 3), the dimerization motif is clearly demarked by the darker fill patterns in Figure 8. The slightly lighter fill pattern in the POPC matrix reflects weaker helix-helix interactions, in accord with a larger inter-helical separation.

The global helix-helix interactions ($H_{inter}$), obtained as a sum over all residue pairs, are given in column 7 of Table 4. Overall, helix-helix inter-

actions are strongly favorable, the unfavorable glycine-glycine interactions being offset by the favorable arrangements of other residues. The inter-helical interactions are roughly −40 kcal/mol, with significant fluctuations of about 3 kcal/mol. Note that in the case of POPC, where the distance between the dimer helices is larger by 1 Å than in DOPC, the helix-helix interaction is weaker by roughly 8 kcal/mol, which is about three times the thermal fluctuation level.

## Helix-environment interaction

If the interaction with the environment is neglected, then only the interaction terms discussed above would be present and would indicate a very strong preference for the dimer form, as measured by the direct helix-helix interaction term $H_{inter}$. Practically, this would correspond to a dimer simulation in vacuum with, presumably, internal restraints to preserve peptide secondary structure. The magnitude of $H_{inter}$ (on the order of −40 kcal/mol) indicates that inter-helical interactions are strongly favorable (attractive), but, as we show next, the interaction of the helix with the lipid bilayer is also highly favorable. The question is then whether the GpA monomer prefers the association with a second helix over complete exposure to lipid molecules. For this reason, the helix-environment interaction term ($H_{env}$) in the dimer simulations is calculated as the sum of the interactions between one helix and lipid, water, and the other helix. That is, the energies are reported on a per monomer basis, regardless of the GpA form, and represent the net interaction between one monomer and everything else in the simulation box.

Table 4 shows that (for the same helical conformations) the monomer interaction with the environment is much lower than in vacuum (by about 200 kcal/mol for the dimer form) due to strong favorable interactions with the lipid bilayer. However, the interaction with the lipid bilayer is such that the total interaction of a GpA helix with the surrounding environment changes by just a small amount going from complete solvation by surrounding lipids (monomer) to having a face exposed to a second helix (dimer). The enthalpy gap, $\Delta H_{env}$, between monomer and dimer forms is

**Table 4.** Trajectory averaged GpA interactions per monomer

| Lipid | $H_{intra}^{nb}$ | | $H_{intra}^{b}$ | | $\Delta H_{intra}$ | $H_{inter}$ | $H_{env}$ | | $\Delta H_{env}$ |
| | Mono | Dimer | Mono | Dimer | | | Mono | Dimer | |
|---|---|---|---|---|---|---|---|---|---|
| DMPC | −80 | −83 | 302 | 302 | −3 | −37.0 (3.0) | −243 | −238 | +5 |
| DPPC | −82 | −83 | 312 | 313 | −0 | −39.5 (3.0) | −228 | −227 | +1 |
| DOPC | −83 | −81 | 299 | 299 | 2 | −36.7 (2.5) | −229 | −239 | −10 |
| POPC | −79 | −76 | 300 | 302 | 5 | −28.6 (2.6) | −235 | −244 | −9 |

$H_{intra}$ (intra-helical), $H_{inter}$ (inter-helical), and $H_{env}$ (net interaction with environment). Contributions from non-bonded (nb) and bonded (b) terms to $H_{intra}$ are given separately. The values in parentheses respresent root-mean-square fluctuations in the inter-helical interaction. The energy units are kcal/mol.
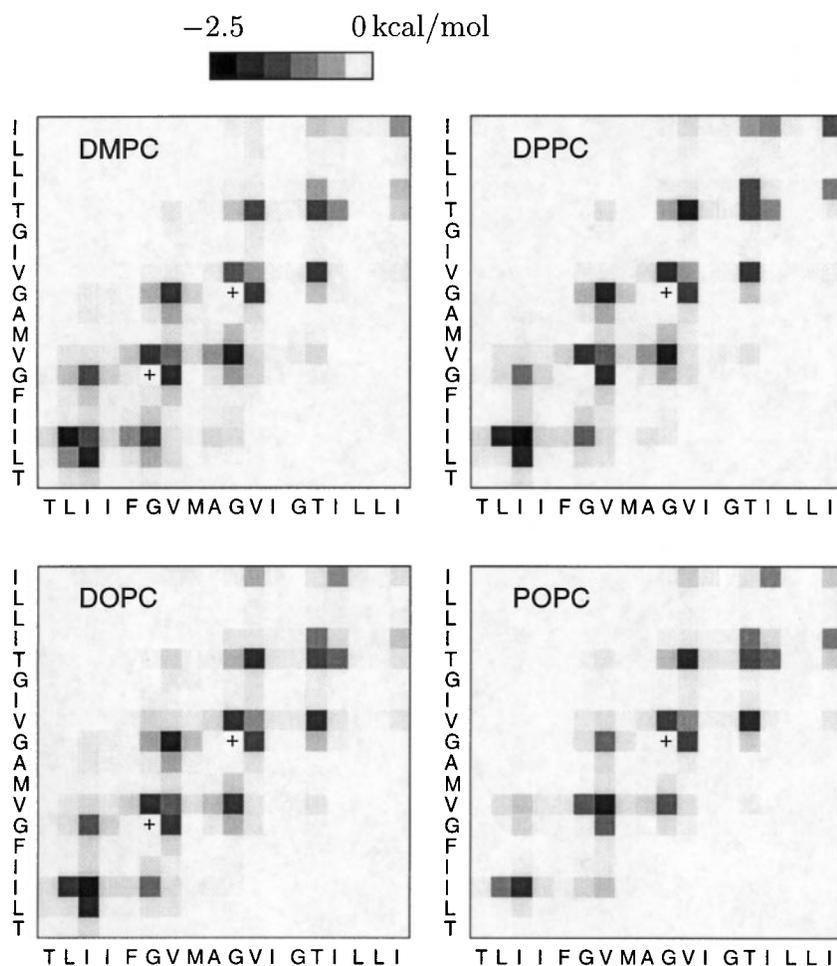
−2.5          0 kcal/mol



**Figure 8.** Trajectory averaged residue-residue interactions. The interaction energies vary from −2.5 kcal/mol (dark fill) to 0 kcal/mol (white fill), except for glycine pairs which interact unfavorably (0.1-0.5 kcal/mol) and which are marked by the plus signs.

much reduced from that in vacuum. The enthalpy gap is in fact reduced to a level where small differences in helical self energies ($\Delta H_{\mathrm{intra}}$) may become significant. Comparing the helix self energies alone, we observe higher energy levels for the dimer/POPC simulation relative to the monomer/POPC.

At this point, a discussion of the possible artifacts in the case of our GpA/POPC simulations is required. A number of structural parameters, including the strong distortion of the N terminus, the larger center of mass separation between the dimer units, together with weaker inter-helical interactions, may indicate artifactual sampling. Note, however, that the POPC simulations are internally consistent: the increase in the GpA self energy in the dimer form relative to the monomer form was accompanied by a larger decrease in the GpA-environment interaction term. In other words, the net helix energy decreases at the (relatively minor) expense of local structural distortion. It is also important to note that, at present there is no accurate experimental data on the area per POPC lipid and the corresponding number of water molecules. Therefore, there is a likely possibility that our choice for these parameters (see Table 6, below) is not optimal.

Examination of the helix-environment interactions ($H_{\mathrm{env}}$) given in Table 4 suggests that upon dimerization, the peptide monomer is driven into a significantly lower enthalpic energy state (dimer *versus* monomer form) in the case of the unsaturated lipids, as opposed to the case of saturated ones. This reflects again the differences in GpA behavior seen in saturated *versus* unsaturated lipids, observed previously in the volume analysis. These differences between the effects of saturated and unsaturated lipids on peptide properties may be related to the higher degree of lipid chain disorder typically present in unsaturated lipid bilayers, as indicated experimentally by measurements on fluid phase lipid bilayers using ${}^{2}$H NMR (Holte *et al.*, 1995), and X-ray scattering (Petrache *et al.*, 1998a).

The range of energy fluctuations can be seen in detail from Figure 9, where we present interaction energies for each monomer unit from the dimer/DMPC trajectories. The interaction between GpA helix and environment is presented in terms of individual contributions from water (c) and lipid (d) interactions, in order to emphasize the different partitioning between the two terms. The fluctuations of the various GpA interaction terms are on the order of 10-20 kcal/mol, which is to be com-
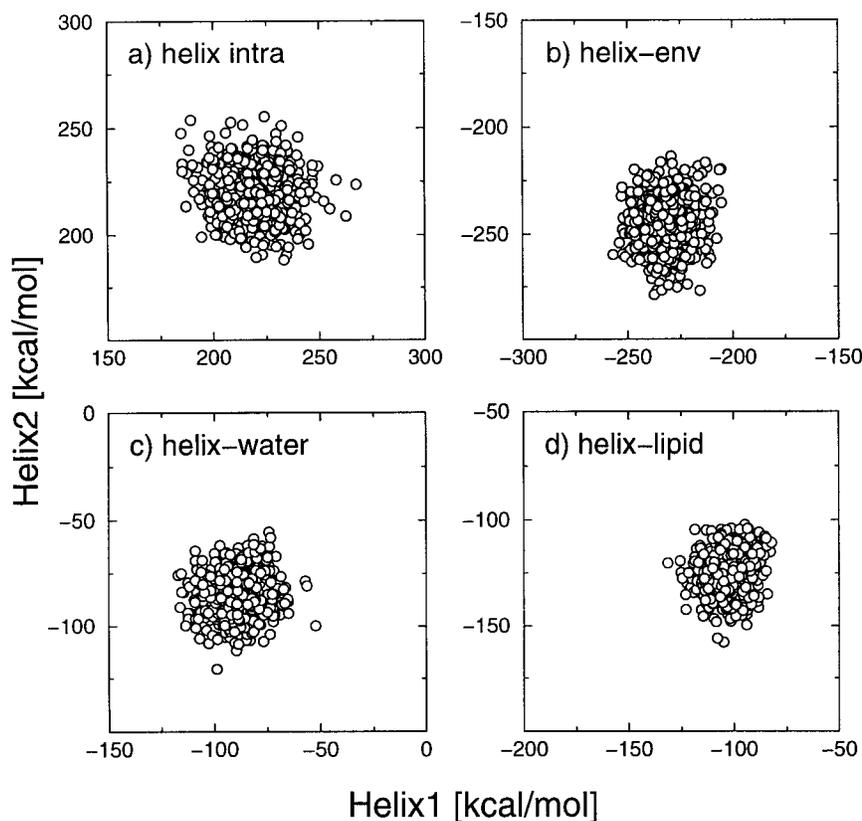
**Figure 9.** Instantaneous intra-helical (a) and helix-environment (b) energy terms for individual GpA monomers in the dimer/DMPC simulations. The values in (b) represent the sum of helix-helix (Table 4), helix-water (c) and helix-lipid (d) energy terms. Note that the energy range on each axis in every panel is the same (150 kcal/mol) for easy comparison of the range of fluctuations of the different energy terms.

pared with 3 kcal/mol in the case of helix-helix interactions. We note that the range of fluctuations in the helix-lipid interaction is slightly narrower than the helix self energy fluctuations.

**Lipid-environment interaction**

As emphasized by White & Wimley (1999), when discussing the energetics of the lipid-peptide systems, the peptide interaction terms are only part of the picture. The analysis of the dimer formation free energy is complex and requires a consistent definition and calculation of enthalpic as well as entropic terms. In addition to the peptide related terms (and apart from entropic contributions that are not calculated here), the energy terms associated with the perturbation of the lipid bilayer need to be taken into account. A direct comparison of the lipid energy terms across the different lipid bilayer types is not warranted, primarily due to the differences in the acyl chain composition. However, the changes in the lipid energy terms upon interaction with the GpA peptide are able to convey information in regard to the bilayer effects on the energetics of the peptide system. The calculated trajectory averaged lipid energies from neat bilayer and GpA/lipid simulations are given in Table 5. The values represent averages over all

lipids in each trajectory. Despite the small magnitude of the effect, there is a clear increment of the lipid energy as the size of the bilayer perturbation increases from neat systems (pure lipid) to lipid-monomer and to lipid-dimer complexes. It is instructive to note that even a small perturbation of the lipid energy states is sufficient to perturb the bilayer thickness significantly (see Table 2). Note that the increased lipid energies would actually disfavor dimer formation, and this result can be taken as an indication that lipid entropic terms, which presumably favor peptide aggregation, play a significant role.

**Boundary lipids**

The boundary lipid concept implies a local change of lipid properties near to the peptide or protein. The precise effect on the lipid molecules, however, and the level of perturbation induced by membrane insertions, are still debated issues. Current experimental techniques do not permit a direct observation of boundary lipids, rather, their existence is inferred from a combination of theory and experimental results (e.g. see Harroun *et al.*, 1999). Simulations, however, have a clear advantage on this issue, even if results may require complex interpretation (Chiu *et al.*, 1999) and may strongly

**Table 5.** Trajectory averaged lipid energies per one lipid molecule

| Lipid | $H_{\text{intra}}^L$ | | | | $H_{\text{env}}^L$ | | | |
|---|---|---|---|---|---|---|---|---|
| | Neat | Mono | Dimer | $\Delta H_{\text{intra}}^L$ | Neat | Mono | Dimer | $\Delta H_{\text{env}}^L$ |
| DMPC | 94.5 | 95.2 | 96.3 | 1.1 | −194.7 | −193.7 | −193.3 | 0.4 |
| DPPC | 108.8 | 110.5 | 110.4 | −0.1 | −197.7 | −199.1 | −196.4 | 2.7 |
| DOPC | - | 119.6 | 119.5 | −0.1 | − | −208.7 | −206.6 | 2.2 |
| POPC | - | 112.3 | 113.1 | 0.8 | - | −206.6 | −205.1 | 1.4 |

$H_{\text{intra}}^L$ (self energy), and $H_{\text{env}}^L$ (net interaction with environment). The energy units are kcal/mol.

depend on the nature of the inserted molecule (Tieleman *et al.*, 1998; Petrache *et al.*, 2000). Indeed, our GpA lipid simulations show that in the vicinity of the peptide, the local bilayer thickness differs from its value away from the peptide, but does so differently for the monomer and for the dimer systems (see Table 2). Developing a detailed description of lipid conformations, especially in the fluid phase, is in general a difficult task and involves the examination of various lipid degrees of freedom, such as internal chain conformations (*trans/gauche* isomerizations) and global chain tilt. This conformational analysis is quite complex and it is not included in this paper. We do, however, include results regarding the energetic aspect of the problem, which may be useful for further understanding and modeling of lipid-protein interactions (Woolf, 1998). Specifically, we plot the lipid self energy ($E_{\text{LS}}$) as a function of its interaction with the GpA peptide ($E_{\text{LG}}$). Figure 10(a) shows a scatter plot of the observed energy states. Each point represents a sampled lipid state in terms of two instantaneous energy terms: $E_{\text{LS}}$ and $E_{\text{LG}}$. For each time frame, every 2 ps, we have recorded the self energy term for each lipid and its interaction with the peptide. The density of points is a measure of conformational sampling; the majority of states, and the higher density of points, is around $E_{\text{LG}} = 0$, representing "bulk lipid" states. The average self energies from the neat bilayer trajectories are also shown in Figure 10(a) with filled symbols, together with 1 and 2 standard deviation bars for easy comparison with the distribution of the $E_{\text{LS}}$ values from the GpA/lipid simulations.

Figure 10(a) shows that, even if bilayer structural properties vary with the distance form the GpA molecule, there is no noticeable effect on the magnitude of the lipid self energies as $E_{\text{LG}}$ becomes stronger. This is, however, not very surprising, since the overall changes of lipid energies are small (as seen in Table 5) it is merely a confirmation that lipid self energies are highly degenerate. Note that even though the average lipid self energy does not depend on $E_{\text{LG}}$, the distribution (width) about the average does. In addition, Figure 10(a) suggests that the population of states along the $E_{\text{LG}}$ dimension is not uniform. In other words, the presence of the GpA peptide may have a strong entropic effect rather than a purely enthalpic effect. Unfortunately, the sampling of various lipid states during our 1.25 ns trajectories, especially for large $E_{\text{LG}}$

values, is not sufficient for a good estimate of these entropic effects.

Given that most of the GpA-lipid interface is located in the lipid hydrocarbon region, we have examined the interaction between the GpA molecule and the individual lipid acyl chains. Figure 10(b) plots the instantaneous interaction (every 2 ps) between each lipid chain (*sn*1 or *sn*2) and the peptide, for all lipids in the simulation box. In these plots, most of the points are off-diagonal. This result indicates that lipid-protein interactions most likely occur through single chains of individual lipids, rather than both lipid chains simultaneously.

## Comparison with Experimental Data

### NMR structure

The starting point for our calculations was the recently determined NMR structure in dodecylphosphocholine micelles by MacKenzie *et al.* (1997). The NMR structure was solved using a set of NOE distance restraints along with *J*-coupling values to limit dihedral angles. The resulting family of structures, determined *via* X-PLOR calculations, represents a well defined transmembrane domain (0.8 Å heavy atom RMS). One important question that arises is whether the structure of the GpA transmembrane domain is in any way different in the dodecylphosphocholine micelles than in planar lipid bilayers. In particular, structural differences would be reflected in the values of hydrogen-hydrogen distances. To address this question, we have first calculated average hydrogen-hydrogen distances from the set of NMR structures, together with their mean square deviations across the set. The hydrogen pairs considered correspond to the assigned NOE signals used as constraints in the NMR structure determination. We then calculated the corresponding hydrogen-hydrogen distances for each of our four dimer trajectories. In the case of chemically equivalent hydrogen atoms we took the minimum distance in each time frame, in order to account for side-chain rotations. The results are presented in Figure 11 and show similar ranges of hydrogen-hydrogen distances in all four bilayer simulations. Compared to the NMR structures, the simulations show larger separations at the N terminus of the transmembrane domain. It is worth noting that the X-PLOR calculations used unrealistic
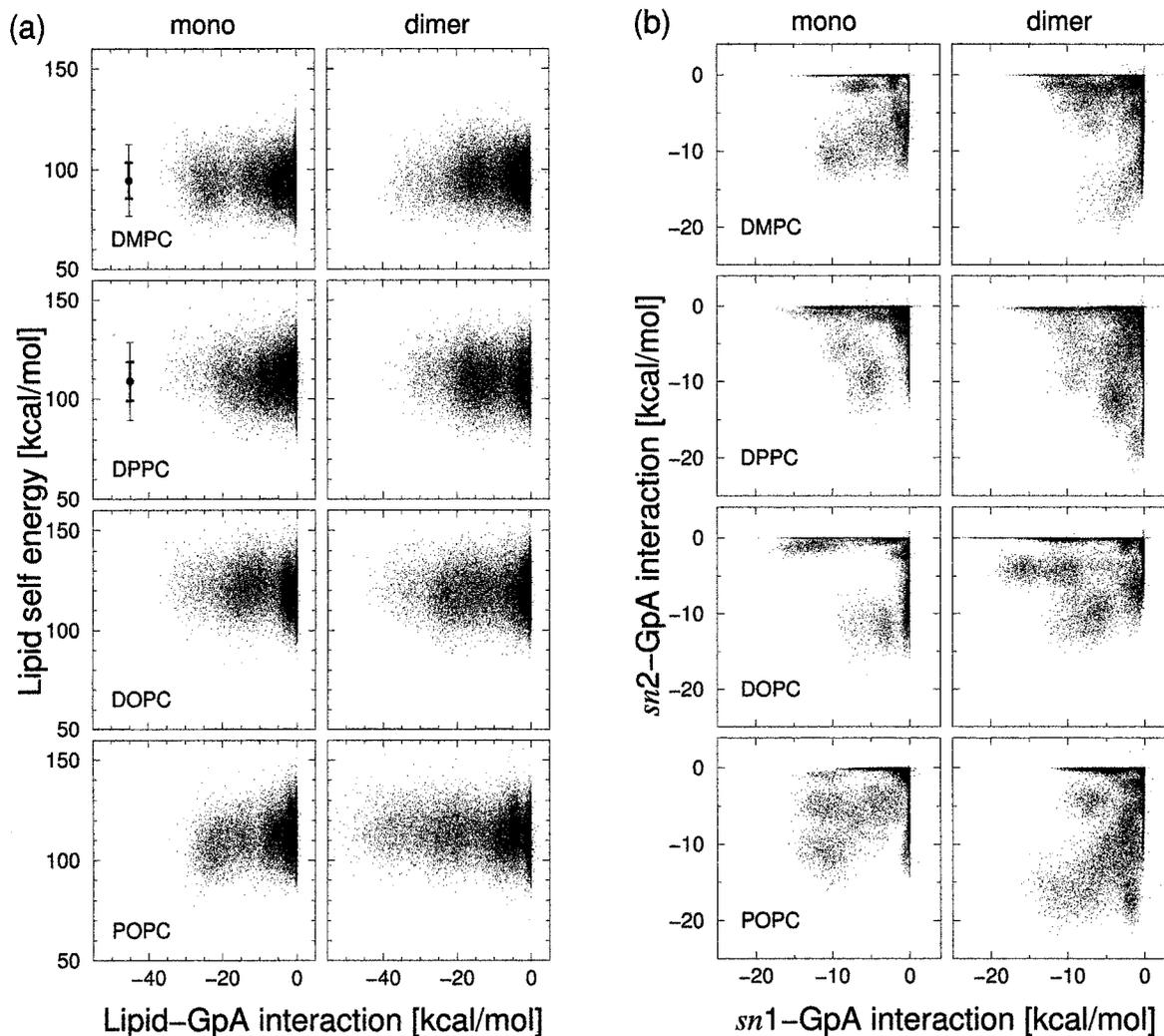
**Figure 10.** (a) Instantaneous (every 2 ps) lipid self energy ($E_{LS}$) *versus* lipid-GpA interaction energy ($E_{LG}$). The average values of $E_{LS}$ from the neat DMPC and DPPC trajectories are shown with filled circle symbols and with $1\sigma$ and $2\sigma$ fluctuation bars. (b) Instantaneous GpA interactions with the *sn1* and the *sn2* acyl chains of the same lipid, for all lipids in each simulation box.

(repulsive only) non-bonded terms, which may generate more rigid structures.

Additional structural information comes from solid-state NMR (rotational resonance) experiments (Smith *et al.*, 1994). One particular result is an average distance of 4.5($\pm$0.5) Å between the $\alpha$-carbon of G83 and the carbonyl carbon of V80, as well as between the $\alpha$-carbon of G83 and the carbonyl carbon of M81 (the experiments were performed on $^2$H-DMPC bilayers at $-50\,^\circ$C). From our trajectories we have calculated average values of 4.5($\pm$0.2) Å for the first, and 4.5($\pm$0.1) Å for the latter distance, where the deviations indicate the RMS fluctuations during the trajectories. The same results were obtained for both monomer and dimer forms, indicating that the region around G83 is very stable in both forms, as has been seen in the behavior of backbone angles (Figure 2). These results further suggest that the range of structures in all four bilayers are consistent with the

measured NMR restraints. Interestingly, we have also calculated the corresponding inter-monomer distances, in addition to the intra-monomer ones reported above, and found very similar results (within the experimental accuracy). The results are 4.7($\pm$0.3) Å for G83-C$^\alpha$ to V80-C, and 6.8($\pm$0.3) Å for G83-C$^\alpha$ to M81-C distances, with slightly larger values in the case of POPC.

In sum, these results imply that the micelle-based structure is valid for the bilayer setting.

## Dimerization motif

An important ingredient in the GpA structure prediction (Treutlein *et al.*, 1992; Adams *et al.*, 1994) has been the result of replacement mutagenesis studies that identified the critical residues involved in GpA dimerization (Lemmon *et al.*, 1992a,b). Additional properties of the GpA dimer interface have been determined based on insertion
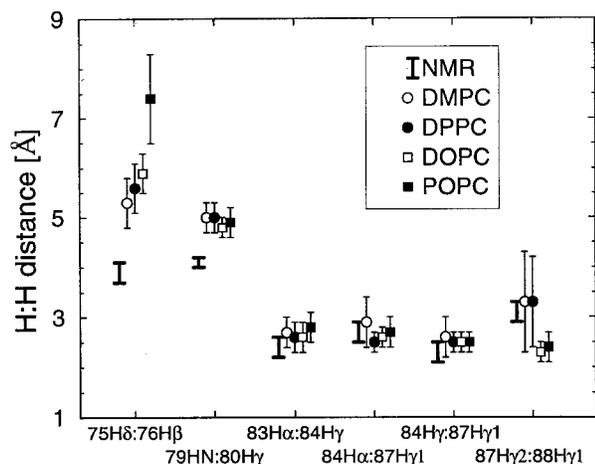
**Figure 11.** H-H distances (among chemically equivalent H atoms) for residue pairs with assigned NOE signals. Averages and fluctuations from the 20 NMR structures are shown with the thick vertical bars. MD results are shown with open circles (DMPC), filled circles (DPPC), open squares (DOPC), and filled squares (POPC), respectively.



**Figure 12.** Trajectory average interaction energies between each residue and the opposed helix in the dimer form. The absolute values are shown in order to emphasize residue importance, as explained in the text. The grey background bars represent the empirical diagram of disruptive effect from Lemmon *et al.* (1992b) (the diagram is scaled by a factor of 2 for a better comparison).

mutagenesis (Mingarro *et al.*, 1996, 1999). In this regard, we have examined our simulation results for possible insights into those residues most critical for dimer stability and thus, presumably, least tolerant of mutations.

It is clear that one relevant property of these critical residues is the interaction strength with the opposite helix. These residue-helix interaction terms are presented in the enthalpy diagram shown in Figure 12. As expected, stronger interactions are obtained for the motif xLIxxGVxxGVxxT. Interestingly, the plot in Figure 12 closely resembles the diagram of disruptive effect of mutagenesis reported by Lemmon *et al.* (1992b). The empirical scale from Lemmon *et al.* is shown by the grey bars in the background of Figure 12.

Note, however, that the enthalpy alone misrepresents the importance of smaller residues, glycines in particular. A mutation from a small residue to a larger one alters the enthalpic contribution, and at the same time, adds a packing strain at the dimer interface. In other words, there is a packing penalty associated with each particular mutation. In addition to the residue interaction strength, a search for critical residues should consider a number of additional parameters as described by MacKenzie & Engelman (1998). Nevertheless, the enthalpy diagram (Figure 12) by itself reproduces the mutagenesis pattern very well.

The present simulations confirmed previous computational and experimental work that suggested the close proximity of Gly83-Gly83 in the dimer interface. In fact, all four simulations showed an unfavorable (positive) interaction
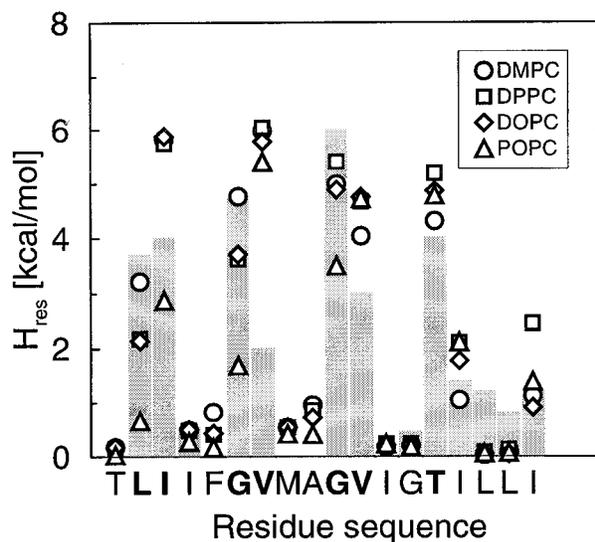
energy between these glycine residues that was compensated by other favorable energy terms between the helices. A possible rationale for this type of molecular interaction was suggested by the analysis of Javadpour *et al.* (1999) on transmembrane protein domains. Their analysis suggested a predominance of glycine residues at many structurally defined helix crossing points. Being the smallest residues, glycines facilitate helix-helix interactions by allowing a close contact between two opposing helices, and thus support a wide range of helix crossing angles (Treutlein *et al.*, 1992; Bowie, 1997). In addition to the role of glycine residues on helix-helix packing, the current simulations indicate that the helix crossing angle depends not only on the properties of the helix-helix interface, but is also coupled to the helix tilt relative to the membrane normal, *via* helix-lipid bilayer interactions.

Recently, the GxxxG pattern has been shown to frequently mediate helix-helix transmembrane associations (Russ & Engelman, 2000; Senes *et al.*, 2000), especially in the presence of β-branched residues at neighboring positions (the pattern is GVxxGV in the case of GpA). Therefore, a detailed analysis of glycine-glycine interactions is in order, especially since the net glycine-glycine interactions appear to be unfavorable, at least in the current CHARMM force fields. As mentioned above, we have found that the repulsive component is due to electrostatic interactions of backbone carbonyls and

the $C^{\alpha}H_2$ groups. Despite their repulsive interactions, the glycine residues seem to accommodate not only the net helix-helix packing, but also the overall packing of the GpA dimer within the lipid environment. Recall that the glycine volumes (the $C^{\alpha}H_2$ groups) are found to be equal to the volume of the lipid methylene groups that surround the GpA dimer, regardless of glycine position relative to the dimer interface.

## Conclusions

In the framework of the two-stage model for helix association, we have analyzed the properties of the dimer and the monomer forms of GpA in lipid bilayers. The interaction analysis, based on enthalpic contributions alone, reveals a delicate balance between various GpA energy terms, and indicates lower dimer energy states in the case of unsaturated lipids. Among the residues that are critical for dimer formation, the glycine residues on the opposed helices interact in an unfavorable fashion. The close packing at these sites, however, facilitates the favorable interaction of the other interfacial residues, leading to an overall helix-helix attraction.

Our simulation results indicate that, among lipid bilayer structural properties, the bilayer thickness has the most influence on the accessible GpA conformations. In accord with the hydrophobic matching hypothesis (Mouritsen & Bloom, 1984), we found that the structure of the peptide-lipid complex is adjusted by an interplay between bilayer thickness and peptide tilt. The effect is most pronounced in the case of DMPC, where the small bilayer thickness leads to a larger helix crossing angle.

The volumetric analysis shows that the peptide accessible volume is conserved upon dimerization, indicating that the GpA monomer packs equally well with the other monomer, as with lipids. More detailed analysis reveals that lipid molecules interact with the GpA peptide through single chains, rather than both chains at once.

The calculations suggest that the four bilayer environments considered do not change the average GpA structure significantly. However, the range of motions and thus fluctuations about the average are modulated by lipid bilayer properties. This supports the idea that biomolecular systems, and in particular, membrane proteins at physiological temperatures, are best described by fluctuations in the range of their accessible structures. In order to understand protein stability, it is especially important to determine the spectrum of structural fluctuations, since this knowledge allows the determination of flexible *versus* rigid subdomains within the protein. Ultimately, this more complete thermodynamic description may help us understand the complex processes underlying protein function as well as aid structure determination.

## Methods

### Ensemble choice

For lipid bilayer systems, the choice of the simulated ensemble together with the appropriate thermodynamic parameters is a delicate issue. One such parameter is the lipid fluid phase cross-sectional area, for which literature data cover a broad range (Nagle *et al.*, 1996). In addition, the lateral area occupied by the peptide itself is not known precisely. Because of these uncertainties, a constant pressure ensemble would be preferable over a constant area simulation, since the bilayer patch dimensions would then be free to adjust and equilibrate during the simulation run. The complication, however, arises from the presence of a surface tension at the lipid water interface (Jähnig, 1996). It has been argued that a membrane patch that consists of just a small number of lipid molecules has a significant surface tension, on the order of 10-50 dyn/cm (Feller & Pastor, 1996; Chiu *et al.*, 1995; for a discussion on this debated issue, also see Tobias *et al.*, 1997). The most appropriate simulation ensemble will then be $N\gamma P_N T$, i.e., constant number of particles ($N$), constant surface tension ($\gamma$), constant normal pressure ($P_N$), and constant temperature ($T$). Unfortunately, the precise value of the surface tension is hard to determine, because it depends on many factors, such as lipid type and system size. Between the two thermodynamic ensembles, each with its own set of advantages and disadvantages, we chose to use the relatively more rigid $NAP_N T$ ensemble as a starting point. The area $A$ of each simulation box has been chosen in a systematic way as explained below. The benefit of constant area ensembles as a first set of simulation runs is twofold. First, molecular packing is expected to equilibrate faster under a fixed area constraint than in a constant surface tension run. Second, having generated a constant area ensemble, the surface tension can be subsequently calculated and used for future constant surface tension runs. Note that even if the lateral area is fixed, the volume of the simulation cell in a $NAP_N T$ run is not; the vertical dimension of the cell is free to fluctuate under the constant normal pressure ($P_N$) constraint, and in consequence, the densities of the different molecular components are free to adjust, eliminating the density artifacts associated with the constant volume simulations.

### Simulation construction

Simulations were performed using CHARMM version 26 (Brooks *et al.*, 1983). Each GpA simulation consists of one monomer or one dimer form of the glycophorin A transmembrane domain, plus 15 lipids per monolayer (30 lipids in total) and the corresponding number of water molecules (see Table 6). Four different lipid types were considered: DMPC (dimyristoyl-phosphatidylcholine), DPPC (dipalmitoyl-phosphatidylcholine), DOPC (dioleoyl-phosphatidylcholine), and POPC (1-palmitoyl-2-oleoyl-phosphatidylcholine). Periodic boundary conditions in all three spatial directions were used, with constant normal pressure ($P_N = 1$ atm) and constant lateral area, with different values for different lipids, as shown in Table 6. All simulations were performed at 30 °C, except the DPPC systems where trajectories were simulated at 50 °C. The number of water molecules in each case was determined starting from experimental data on fully hydrated multilamellar vesicles of pure lipid bilayers. Specifically, using the number of water molecules per lipid and the lipid cross-sectional area in

**Table 6.** Simulation setup

| Lipid | Area/lipid | Waters/lipid | Total area | | | Total waters | | |
|---|---|---|---|---|---|---|---|---|
| | | | Neat | Mono | Dimer | Neat | Mono | Dimer |
| DMPC[a] | 59.8 | 25.7 | 1075 | 1073 | 1248 | 925 | 924 | 1151 |
| DPPC[b] | 62.9 | 29.1 | 1132 | 1121 | 1296 | 1048 | 965 | 1195 |
| DOPC[c] | 72.2 | 32.5 | - | 1260 | 1436 | - | 1134 | 1293 |
| POPC[d] | 63.0 | 30.0 | - | 1122 | 1298 | - | 1069 | 1236 |

GpA simulations contain 30 lipids, and neat bilayer simulations contain 36 lipids. The area units are $Å^2$.
[a] Petrache *et al*. (1998a).
[b] Nagle *et al*. (1996).
[c] Tristram-Nagle *et al*. (1998).
[d] Estimate.

each lipid bilayer, the number of water molecules per unit area was calculated and then scaled to the total area of the simulation box. (Note the implicit assumption that inter-lamellar water spacing does not change with peptide insertion, which is clearly an approximation. The rationale, however, is based on inter-bilayer interaction studies (Petrache *et al*., 1998b) which show that the water spacing decreases in the absence of bilayer fluctuations. Therefore, using data from fully hydrated, unstressed samples at most overestimates the number of water molecules required to fully hydrate a small, non-fluctuating bilayer patch.) The total area of the simulation box includes the peptide cross-sectional area, and was estimated as follows. First, the volumes for both GpA monomer and dimer were estimated by calculating the excluded volume for a spherical probe the size of a water molecule. These volumes were then divided by effective helix lengths to obtain "bare" cross-sectional areas. Tilt averaged areas were estimated by considering a uniform population of peptide tilt angles between 0 and 25 degrees (Bowie, 1997). These results were combined with the "collapsed" area obtained by translating all atoms along the helix axis in the $z = 0$ plane. Estimated values of $\sim177$ $Å^2$ for the monomer, and $\sim353$ $Å^2$ for the dimer form were used. To these results we then added the area per lipid measured experimentally at full hydration, to obtain the total area of each simulation box. In parallel, we performed neat DMPC and DPPC bilayer simulations, with 18 lipids per monolayer (total of 36 lipids each). Table 1 summarizes all structural information regarding the molecular dynamics setup.

Initial membrane structures were constructed using the procedure proposed by Woolf & Roux (1994, 1996). The NMR structure of GpA (residues 74 to 91) reported by MacKenzie *et al*. (1997) was used as a starting point. Lipid molecules were randomly chosen from pre-equilibrated lipid libraries. The DPPC library was provided by Hardy & Pastor (1994), and also used to generate DMPC molecules by deletion of two terminal carbon segments from each acyl chain. DOPC and POPC libraries were provided by Scott Feller (Armen *et al*., 1998). The lipid placement around the peptide was first determined by a 100 ps simulation of large van der Waals (vdW) spheres constrained in the vicinity of two parallel planes at the average location of the lipid headgroups. Next, lipid molecules were randomly chosen from the libraries and placed at the location of the vdW spheres. The lipids were then systematically rotated and translated around the initial positions, in order to reduce the number of steric collisions, followed by a gradual increase of the vdW atom radii and minimization. During this minimization stage, the peptide atoms were kept fixed to their initial locations, and the lipid glycerol C2 atoms were restrained to their initial plane using a harmonic potential of 10 kcal mol$^{-1}$ Å$^{-2}$ and a drop off cutoff of 1 Å. Next, a TIP3 water overlay was performed from the glycerol regions on both sides of the membrane. For each trajectory, the $z$-dimension of the box was determined by the target number of water molecules chosen in Table 6. Water-lipid packing was first relaxed by a series of minimization and Langevin dynamics simulations, followed by velocity scaling simulations with electrostatics shifted and van der Waals switched at 12 Å. At this stage, the constraints on the peptide and the lipid glycerol atoms were kept on. Next, the constraints on the lipid glycerols were removed, and equilibration continued with 25 ps of leapfrog constant pressure and constant temperature dynamics. In the next stage of equilibration, the peptide restraints were also removed and 25 ps of dynamics were performed using the particle mesh Ewald method for electrostatic interactions (Sagui & Darden, 1999). A cutoff of 12 Å was used for van der Waals interactions (Feller & Pastor, 1999). The time step was 2 fs, and all bonds involving hydrogen atoms were fixed using the SHAKE algorithm, with a tolerance (relative deviation) of $10^{-6}$. The frequency of regenerating the non-bonded list used the heuristic testing algorithm that updates based on the distance each atom moved since the last list update. Production dynamics simulations were performed for 1.5 ns. The results reported in this paper are based on the last 1.25 ns of dynamics, after a 250 ps equilibration window.

## Voronoi procedure

A detailed description of the algorithm used is given by Gerstein *et al*. (1995). Briefly, given a distribution of atoms, the standard Voronoi procedure constructs a polyhedron around each atom, that has the property that all interior points are closer to the central atom than to any others. The resulting partitioning fills the entire space in the simulation box (i.e. allows no voids). The polyhedron faces are located midway between neighboring atoms, which assumes that all atoms have intrinsically the same size. Gerstein *et al*. (1995) have considered more physical partitioning methods to account for atom size differences within a molecular system, such as a protein. These methods calculate the location of the dividing planes based on proportionality relations with the atom van der Waals radii. The authors suggest their method B as most appropriate dividing procedure, which we have used. It was noted that this procedure introduces a "vertex error" at the intersection of three or more dividing planes, but estimates the error to be small. We should also mention that the method uses

heavy atoms only (hydrogen atoms are accounted for implicitly), and may introduce additional errors. Since our main purpose is to estimate volume differences between the GpA peptides in different environments, we expect that these systematic errors do not influence the results significantly.

## Acknowledgments

## References

Adams, P. D., Engelman, D. M. & Brünger, A. T. (1996). An improved prediction for the structure of the dimeric transmembrane domain of glycophorin A obtained through global searching. *Proteins: Struct. Funct. Genet.* **26**, 257-261.

Armen, R. S., Uitto, O. D. & Feller, S. E. (1998). Phospholipid component volumes: determination and application to bilayer structure calculations. *Biophys. J.* **75**, 734-744.

Bezrukov, S. M., Rand, P. R., Vodyanoy, I. & Parsegian, V. A. (1998). Lipid packing stress and polypeptide aggregation: alamethicin channel probed by proton titration of lipid charge. *Faraday Discuss.* **111**, 173-183.

Bormann, B. J. & Engelman, D. M. (1992). Intramembrane helix-helix association in oligomerization and transmembrane signaling. *Annu. Rev. Biophys. Biomol. Struct.* **21**, 223-242.

Bowie, J. U. (1997). Helix packing in membrane proteins. *J. Mol. Biol.* **5**, 780-789.

Brooks, B. R., Bruccoleri, R. E., Olafson, B. D., States, D. J., Swaminathan, S. & Karplus, M. (1983). Charmm: a program for macromolecular energy minimization and dynamics calculations. *J. Comp. Chem.* **4**, 187-217.

Brooks, C. L., Karplus, M. & Pettitt, B. M. (1988). Proteins: a theoretical perspective of dynamics, structure, and thermodynamics. *Advan. Chem. Phys.* **71**, 259.

Brown, M. F. (1994). Modulation of rhodopsin function by properties of the membrane bilayer. *Chem. Phys. Lipids,* **74**, 159-180.

Chiu, S.-W., Clark, M., Balaji, V., Subramaniam, S., Scott, H. L. & Jakobsson, E. (1995). Incorporation of surface tension into molecular dynamics simulation of an interface: a fluid phase lipid bilayer membrane. *Biophys. J.* **69**, 1230-1245.

Chiu, S.-W., Subramaniam, S. & Jakobsson, E. (1999). Simulation study of a gramicidin/lipid bilayer system in excess water and lipid. I. Structure of the molecular complex. *Biophys. J.* **76**, 1929-1938.

Chothia, C., Levitt, M. & Richardson, D. (1981). Helix to helix packing in proteins. *J. Mol. Biol.* **145**, 215-250.

de Planque, M. R. R., Greathouse, D. V., Koeppe, R. E., Schafer, H., Marsh, D. & Killian, J. A. (1998). Influence of lipid/peptide hydrophobic mismatch on the thickness of diacylphosphatidylcholine bilayers. A ²H NMR and ESR study using designed transmembrane α-helical peptides and gramicidin A. *Biochemistry,* **37**, 9333-9345.

Engelman, D. M. & Steitz, T. A. (1981). The spontaneous insertion of proteins into and across membranes - the helical hairpin hypothesis. *Cell,* **23**, 411-422.

Edholm, O., Berger, O. & Jänig, F. (1995). Structure and fluctuations of bacteriorhodopsin in the purple membrane: a molecular dynamics study. *J. Mol. Biol.* **250**, 94-111.

Epand, R. M. (1998). Lipid polymorphism and protein-lipid interactions. *Biochim. Biophys. Acta Rev. Biomembranes,* **1376**, 353-368.

Feller, S. E. & Pastor, R. W. (1996). On simulating lipid bilayers with an applied surface tension: periodic boundary conditions and undulations. *Biophys. J.* **71**, 1350-1355.

Feller, S. E. & Pastor, R. W. (1999). Constant surface tension simulations of lipid bilayers: the sensitivity of surface areas and compressibilities. *J. Chem. Phys.* **111**, 1281-1287.

Feller, S. E., Venable, R. M. & Pastor, R. W. (1997). Computer simulations of a DPPC phospholipid bilayer: structural changes as a function of molecular surface area. *Langmuir,* **13**, 6555-6561.

Fu, R. & Cross, T. A. (1999). Solid-state nuclear magnetic resonance investigation of protein and polypeptide structure. *Annu. Rev. Biophys. Biomol. Struct.* **28**, 235-268.

Gawrisch, K., Han, K.-H., Yang, J.-S., Bergelson, L. D. & Ferretti, J. A. (1993). Interaction of peptide fragment 828-848 of the envelope glycoprotein of human immunodeficiency virus type I with lipid bilayers. *Biochemistry,* **32**, 3112-3118.

Gerstein, M., Tsai, J. & Levitt, M. (1995). The volume of atoms on the protein surface: calculated from simulation, using Voronoi polyhedra. *J. Mol. Biol.* **249**, 955-966.

Greathouse, D. V., Hinton, J. F., Kim, K. S. & Koeppe, R. E., II (1994). Gramicidin A/short-chain phospholipid dispersions: chain length dependence of gramicidin conformation and lipid organization. *Biochemistry,* **33**, 4291-4299.

Hardy, B. J. & Pator, R. W. (1994). Conformational sampling of hydrocarbon and lipid chains in an orienting potential. *J. Comput. Chem.* **15**, 208-226.

Harroun, T. A., Heller, W. T., Weiss, T. M., Yang, L. & Huang, H. W. (1999). Experimental evidence for hydrophobic matching and membrane-mediated interactions in lipid bilayers containing gramicidin. *Biophys. J.* **76**, 937-945.

Holte, L. L., Peter, S. A., Sinnwell, T. M. & Gawrisch, K. (1995). ²H nuclear magnetic resonance order parameter profiles suggest a change of molecular shape for phosphatidylcholines containing a polyunsaturated acyl-chain. *Biophys. J.* **68**, 2396-2403.

Jähnig, F. (1996). What is the surface tension of a lipid bilayer membrane? *Biophys. J.* **71**, 1348-1349.

Javadpour, M. M., Eilers, M., Groesbeek, M. & Smith, S. O. (1999). Helix packing in polytopic membrane proteins: role of glycine in transmembrane helix association. *Biophys. J.* **77**, 1609-1618.

Jost, P. C., Griffith, O. H., Capaldi, R. A. & Vanderkooi, G. (1973). Evidence for boundary lipid in membranes. *Proc. Natl Acad. Sci. USA,* **70**, 480-484.

Keller, S. L., Gruner, S. M. & Gawrisch, K. (1996). Small concentrations of alamethicin induce a cubic phase

in bulk phosphatidylethanolamine mixtures. *Biochim. Biophys. Acta,* **1278**, 241-246.

Killian, J. A. (1998). Hydrophobic mismatch between proteins and lipids in membranes. *Biochim. Biophys. Acta,* **1376**, 401-416.

Koeppe, R. E., II & Andersen, O. S. (1996). Engineering the gramicidin channel. *Annu. Rev. Biophys. Biomol. Struct.* **25**, 231-258.

Kovacs, H., Mark, A. E., Johansson, J. & van Gunsteren, W. F. (1995). The effect of environment on the molecular dynamics simulations of surfactant protein C in chloroform, methanol and water. *J. Mol. Biol.* **247**, 808-822.

Lemmon, M. A. & Engelman, D. M. (1994). Specificity and promiscuity in membrane helix interactions. *FEBS Letters,* **346**, 17-20.

Lemmon, M. A., Flanagan, J. M., Hunt, J. F., Adair, B. D., Bormann, B.-J., Dempsey, C. E. & Engelman, D. M. (1992a). Glycophorin A dimerization is driven by specific interactions between transmembrane α-helices. *J. Biol. Chem.* **267**, 7683-7689.

Lemmon, M. A., Flanagan, J. M., Treutlein, H. R., Zhang, J. & Engelman, D. M. (1992b). Sequence specificity in the dimerization of transmembrane α-helices. *Biochemistry,* **31**, 12719-12725.

Lewis, B. A. & Engelman, D. M. (1983). Lipid bilayer thickness varies linearly with acyl chain length in fluid phosphatidylcholine vesicles. *J. Mol. Biol.* **166**, 211-217.

Litman, B. J. & Mitchell, D. C. (1996). A role for phospholipid polyunsaturation in modulating membrane protein function. *Lipids,* **31**, S193-S197.

MacKenzie, K. R. & Engelman, D. M. (1998). Structure-based prediction of the stability of transmembrane helix-helix interactions: the sequence dependence of glycophorin A dimerization. *Proc. Natl Acad. Sci. USA,* **95**, 3583-3590.

MacKenzie, K. R., Prestegard, J. H. & Engelman, D. M. (1997). A transmembrane helix dimer: structure and implications. *Science,* **276**, 131-133.

Mingarro, I., Whitley, P., Lemmon, M. A. & von Heijne, G. (1996). Ala-insertion scanning mutagenesis of the glycophorin A transmembrane helix: a rapid way to map helix-helix interactions in integral membrane proteins. *Protein Sci.* **5**, 1339-1341.

Mingarro, I., Elofsson, A. & von Heijne, G. (1999). Helix-helix packing in a membrane-like environment. *J. Mol. Biol.* **272**, 633-641.

Mouritsen, O. G. & Bloom, M. (1984). Mattress model of lipid-protein interactions in membranes. *Biophys. J.* **46**, 141-153.

Nagle, J. F. & Wilkinson, D. A. (1978). Lecithin bilayers: density measurements and molecular interactions. *Biophys. J.* **23**, 159-175.

Nagle, J. F., Zhang, R., Tristram-Nagle, S., Sun, W.-J., Petrache, H. I. & Suter, R. M. (1996). X-ray structure determination of fully hydrated $L_\alpha$ phase DPPC bilayers. *Biophys. J.* **70**, 1419-1431.

Novotny, J., Bruccoleri, R. & Karplus, M. (1984). An analysis of incorrectly folded protein models: implications for structure prediction. *J. Mol. Biol.* **177**, 787-818.

Petrache, H. I., Feller, S. E. & Nagle, J. F. (1997). Determination of component volumes from simulations. *Biophys. J.* **72**, 2237-2242.

Petrache, H. I., Tristram-Nagle, S. & Nagle, J. F. (1998a). Fluid phase structure of EPC and DMPC bilayers. *Chem. Phys. Lipids,* **95**, 83-94.

Petrache, H. I., Gouliaev, N., Tristram-Nagle, S., Zhang, R., Suter, R. M. & Nagle, J. F. (1998b). Interbilayer interactions from high-resolution X-ray scattering. *Phys. Rev. E,* **57**, 7014-7024.

Petrache, H. I., Killian, J. A., Koeppe, R. E., II & Woolf, T. B. (2000). Interaction of WALP peptides with lipid bilayers: molecular dynamics simulations. *Biophys. J.* **78**, 324A.

Pink, D. A., Georgallas, A. & Chapman, D. (1981). Intrinsic proteins and their effect upon lipid hydrocarbon chain order. *Biochemistry,* **20**, 7152-7157.

Popot, J.-L. & Engelman, D. M. (1990). Membrane protein folding and oligomerization: the two-stage model. *Biochemistry,* **29**, 4031-4037.

Rehorek, M., Dencher, N. A. & Heyn, M. P. (1985). Long-range lipid-protein interactions. Evidence from time-resolved fluorescence depolarization and energy-trasfer experiments with bacteriorhodopsin-dimyristoylphosphatidylcholine vesicles. *Biochemistry,* **24**, 5980-5988.

Richards, F. M. (1985). Calculation of molecular volumes and areas for structures of known geometry. *Methods Enzymol.* **115**, 440-464.

Roux, B. & Woolf, T. B. (1996). Molecular dynamics of Pf1 coat protein in a phospholipid bilayer. In *Biological Membranes: A Molecular Perspective from Computation and Experiment* (Merz, K. M. & Roux, B., eds), pp. 555-587, Birkhauser Press, Boston.

Russ, W. P. & Engelman, D. M. (2000). The GxxxG motif: a framework for transmembrane helix-helix association. *J. Mol. Biol.* **296**, 911-919.

Sagui, C. & Darden, T. A. (1999). Molecular dynamics simulations of biomolecules: long-range electrostatic effects. *Annu. Rev. Biophys. Biom.* **28**, 155-179.

Shen, L., Bassolino, D. & Stouch, T. (1997). Transmembrane helix structure, dynamics, and interactions: multi-nanosecond molecular dynamics simulations. *Biophys. J.* **73**, 3-20.

Senes, A., Gerstein, M. & Engelman, D. M. (2000). Statistical analysis of amino acid patterns in transmembrane helices: the GxxxG motif occurs frequently and in association with β-branched residues at neighboring positions. *J. Mol. Biol.* **296**, 921-936.

Smith, S. O., Jonas, R., Braiman, M. & Bormann, B. J. (1994). Structure and orientation of the transmembrane domain of glycophorin A in lipid bilayers. *Biochemistry,* **33**, 6334-6341.

Sperotto, M. M. & Mouritsen, O. G. (1991). Monte-Carlo simulations studies of lipid order parameter profiles near integral membrane proteins. *Biophys. J.* **59**, 261-270.

Tieleman, P. D., Forrest, L. R., Sansom, M. S. P. & Berendsen, H. J. C. (1998). Lipid properties and the orientation of aromatic residues in OmpF, influenza M2, and alamethicin systems: molecular dynamics simulations. *Biochemistry,* **37**, 17554-17561.

Tobias, D. J., Tu, K. C. & Klein, M. L. (1997). Atomic-scale molecular dynamics simulations of lipid membranes. *Curr. Opin. Colloid Inr.* **2**, 15-26.

Treutlein, H. R., Lemmon, M. A., Engelman, D. M. & Brünger, A. T. (1992). The glycophorin A transmembrane domain dimer: sequence-specific propensity for a right-handed supercoil of helices. *Biochemistry,* **31**, 12726-12732.

Tristram-Nagle, S., Petrache, H. I. & Nagle, J. F. (1998). Structure and interactions of fully hydrated dioleoylphosphatidylcholine bilayers. *Biophys. J.* **75**, 917-925.

White, S. H. & Wimley, W. C. (1999). Membrane protein folding and stability: physical principles. *Annu. Rev. Biophys. Biom.* **28**, 319-365.

Wiener, M. C. & White, S. H. (1992). Structure of fluid DOPC determined by joint refinement of X-ray and neutron diffraction data. III: complete structure. *Biophys. J.* **61**, 434-447.

Woolf, T. B. (1997). Molecular dynamics of individual α-helices of bacteriorhodopsin in dimyristoylphosphatidylcholine. I. Structure and dynamics. *Biophys. J.* **73**, 2376-2392.

Woolf, T. B. (1998). Molecular dynamics of individual α-helices of bacteriorhodopsin in dimyristoylphosphatidylcholine. II. Interaction energy analysis. *Biophys. J.* **74**, 115-131.

Woolf, T. B. & Roux, B. (1994). Molecular dynamics simulation of the gramicidin channel in a phospholipid bilayer. *Proc. Natl Acad. Sci. USA,* **91**, 11631-11635.

Woolf, T. B. & Roux, B. (1996). Structure, energetics and dynamics of lipid-protein interactions: a molecular dynamics study of the gramicidin a channel in a DMPC bilayer. *Proteins: Struct. Funct. Genet.* **24**, 92-114.

Yau, W.-M., Wimley, W. C., Gawrisch, K. & White, S. H. (1998). The preference of tryptophan for membrane interfaces. *Biochemistry,* **37**, 14713-14718.

Zhang, Y. H., Feller, S. E., Brooks, B. R. & Pastor, R. W. (1995). Computer simulations of liquid/liquid interfaces. 1. Theory and applications to octane/water. *J. Chem. Phys.* **103**, 10252-10266.

*Edited by G. Von Heijne*